Available online at www.sciencedirect.com

ScienceDirect

Procedia Structural Integrity 24 (2019) 251–258

Structural Integrity Procedia

www.elsevier.com/locate/procedia

AIAS 2019 International Conference on Stress Analysis

Adhesion of compliant spheres: an experimental investigation

Guido Violano[a], Luciano Afferrante[a,1]

[a]*Department of Mechanics, Mathematics and Management, Polytechnic University of Bari, Via Re David, 200, 70124, Bari, Italy*

Abstract

The detachment of soft adhesive spheres is strongly affected by the displacement rate. Nonetheless, the classical Johnson, Kendall & Roberts (JKR) theory is usually adopted to describe both the loading and unloading process, with the implicit assumption of defining different values of the elastic modulus and interfacial adhesion energy for the two phases.

In this work, we use a different approach to model the unloading phase, usually characterized by viscoelastic dissipation. Specifically, experimental data are fitted with the numerical model proposed by Muller for the contact of viscoelastic spheres. In such way, by exploiting a mixed JKR-Muller model, we are able to quantify the energy loss due to elastic and viscoleastic adhesion hysteresis.

Moreover, we find that the pull-off force is order of magnitude larger than the JKR prediction and increases with the detachment rate, while the effect of the maximum load reached before unloading is, as expected, negligible.

Keywords: Viscoelasticity; adhesion hysteresis; JKR theory

1. Introduction

Johnson, Kendall & Roberts (JKR) (Johnson et al., 1971) firstly investigated the adhesive contact of two elastic spheres of radii R_1 and R_2. They found the pull-off force, i.e. the force required to separate the contacting spheres, to be equal to $1.5\pi R\Delta\gamma_0$, being R the equivalent radius ($1/R = 1/R_1 + 1/R_2$) and $\Delta\gamma_0$ the interfacial surface energy. Afterwards, Derjaguin, Muller & Toporov (DMT) (Derjaguin et al., 1975) proposed a different model and predicted a pull-off force $2\pi R\Delta\gamma_0$. Prefactor apart, both JKR and DMT theories lead to a pull-off force which depends exclusively on the geometry and adhesion energy of the contacting bodies.

Different studies proved that the pull-off force is instead dependent also on the elastic properties of the materials (Greenwood, 1997; Ciavarella et al., 2017). Such dependence is described through the so-called Tabor parameter

* Corresponding author. Tel.: +39 080 5962704.
E-mail address: luciano.afferrante@poliba.it

10.1016/j.prostr.2020.02.022

$\mu = \left[R\Delta\gamma_0^2/(E^{*2}\epsilon^3)\right]^{1/3}$ (Tabor, 1977) , where ϵ is the range of attractive forces (of the order of atomic spacing) and E^* is the composite elastic modulus of the contacting spheres. DMT theory applies for hard elastic materials and long range adhesive interactions ($\mu \ll 1$), while JKR theory is exact in the limit of short range adhesive forces and soft elastic bodies ($\mu \gg 1$).

In DMT and JKR theories the contact is assumed to be broken at low velocity, under quasi-static conditions. However, in many experiments of contact between elastomers, the pull-off process unlikely obeys the quasi-static conditions (Maugis and Barquins, 1980; Greenwood and Johnson, 1981; Tiwari et al., 2017). Elastomers are characterized by a strong dependence of the effective work of adhesion $\Delta\gamma$ on the velocity v_p of the contact line.

Moving from a generalization of the JKR theory, Maugis & Barquins (MB) showed that the dependence of $\Delta\gamma$ on v_p can be expressed in terms of a dissipation function related exclusively to the viscoelastic properties of the material (Maugis and Barquins, 1980). In their formulation, MB made the assumption that viscoelastic losses are located at the edge of the contact. This condition entails that *"gross displacements must be elastic for G to be valid in kinetic phenomena"*, where G is the amount of energy required to advance a fracture plane by a unit area and, hence, characterizes the strength of adhesion.

Also, Muller (1999) showed that the process of detachment can be described by a first-order differential equation, whose solution is based on the MB assumption, according to which viscoelastic losses do not involve bulk deformations. This assumption would fail in presence of sliding (Menga et al., 2018a; Menga et al., 2018b; Afferrante et al., 2019; Putignano et al., 2019).

Understanding the origin of the hysteretic behavior usually observed during detachment experiments of compliant bodies is not simple, since it may be due to multiple causes, such as elastic instability (Greenwood, 1997; Attard, 2000), viscoelasticity (Maugis and Barquins, 1980; Giri et al., 1972; Lorenz et al., 2013; Afferrante and Carbone 2016), plasticity (Oliver et al., 1992), processes related to material chemistry (Maeda et al., 2002; Chen et al., 2005) and even molecular entanglement (Cross et al., 2006).

In this work we focus on two causes: elastic instabilities and viscoelasticity.

In the case of very soft and compliant materials, jump-on and jump-off contact instabilities characterize the loading and unloading phases, respectively. With reference to Fig. 1, where the force-approach relation is sketched, the loading-unloading path predicted by the JKR theory is plotted with black line. Under displacement controlled conditions and according to JKR theory, during loading phase jump to contact occurs when the approach δ is equal to zero. During unloading, if we neglect viscous effects, the force-approach relation follows the same curve. However, unstable detachment occurs at negative δ when the approach reduces up to the jump-off value δ_{OFF}. The yellow area represents the hysteretic energy loss related to elastic instabilities (denoted as energy lost for Elastic Adhesion Hysteresis, EAH). It is exclusively influenced by the geometrical, elastic and adhesive properties of the contacting bodies. Several works (Greenwood, 1997; Ciavarella et al., 2017; Attard, 2000) showed that, in the contact of spheres, EAH increases with the Tabor parameter μ, while negligible hysteretic losses occur when $\mu \to 0$. In the latter case, DMT theory is largely accurate in estimating adhesion.

However, in contact experiments involving elastomers, the unloading curve is usually found not coinciding with the loading one due to viscoelastic losses detected during the detachment process (red line in Fig. 1). In such case, the energy loss related to the viscoelastic dissipation (denoted as energy lost for Viscoelastic Adhesion Hysteresis, VAH) is represented by the gray area and the pull-off process is rate-dependent, since the unloading path is strongly influenced by the velocity of the contact line v_p.

Such typical behavior is found in our experimental investigations, also at very low detachment velocities. However, on the contrary of previus works, where experimental data are usually fitted according to the JKR theory by defining equivalent values for E^* and $\Delta\gamma_0$ in the loading and unloading phases (Tiwari et al., 2017; Dorogin et al., 2017), here we propose a different approach. JKR theory is exploited to fit data measured during loading, where viscoelastic effects are clearly negligible; the unloading phase is then described according to the Muller numerical solution (Muller, 1999). Such an approach allows to distinguish the energy loss due to elastic instabilities and viscoelastic dissipation.

Moreover, the present approach could be exploited in multiasperity theories, like those proposed by Afferrante et al. (2012), Afferrante et al. (2018), Violano et al. (2018), Violano and Afferrante (2019a), Violano and Afferrante (2019b) for a more accurate description of the attachment and detachment processes of compliant bodies with rough surface (Yashima et al., 2015; Acito et al., 2019).

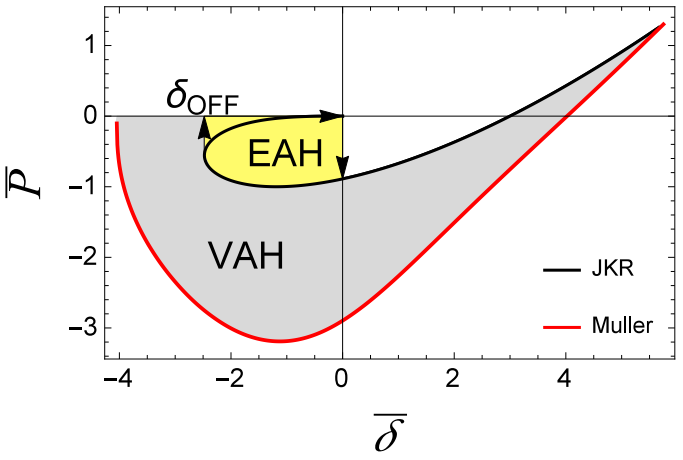

Fig. 1: The force vs penetration relation predicted by the JKR theory (black solid line) for a single asperity contact. The red solid line represents the unloading path predicted by Muller model. The yellow and gray areas are the EAH and VAH contributions respectively.

2. Detachment of viscoelastic spheres

Moving from the basic relations of JKR theory, Muller (1999) proposed a numerical approach to describe the detachment process of a viscoelastic sphere from a rigid half-space.

Under the assumption of a constant pull-off rate, for a sphere of radius R in contact over a circular area of radius a, Muller proposed a two-parameter equation to include the effect of viscoelasticity in the detachment process

$$\frac{d\bar{a}}{d\bar{\delta}} = \frac{1}{\beta}\left[\bar{a}^3\left(1-\frac{\bar{\delta}}{3\bar{a}^2}\right)^2 - \frac{4}{9}\right]^{1/n} \tag{1}$$

where we have defined the following dimensionless quantities $\bar{a} = a/a_0$ and $\bar{\delta} = \delta/\delta_0$,with $a_0 = 3R\left[\pi\Delta\gamma_0/(6E^*R)\right]^{1/3}$ and $\delta_0 = R\left[\pi\Delta\gamma_0/(6E^*R)\right]^{2/3}$.

In eq. (1), β is a parameter depending on the viscoelastic and adhesive properties of the bodies, and it is proportional to the pull-off rate $V = -d\delta/dt$. The second parameter n is a characteristic constant of the elastomer, and it may be determined experimentally. In general, n ranges from 0.1 to 0.8.

The classical JKR equations relating load, contact radius and approach can be rewritten in dimensionless form as

$$\bar{a} = \left\{\frac{1}{2}\left[1+\left(1+\bar{P}\right)^{1/2}\right]\right\}^{2/3} \tag{2}$$

$$\bar{\delta} = \left(\bar{a}^2 + \frac{\bar{P}}{2\bar{a}}\right) \tag{3}$$

where $\bar{P} = P/P_0$, with $P_0 = 1.5\pi R\Delta\gamma_0$.

Given the load P_i reached at the end of the loading process, eqs. (2) and (3) can be used to calculate the values of the contact radius a_i and penetration δ_i at the beginning of the unloading phase.

With these initial conditions, eq. (1) can be solved to obtain the contact radius vs penetration relation. The dimensionless contact load is then calculated by

$$\bar{P} = 2\bar{a}\left(\bar{\delta} - \bar{a}^2\right). \tag{4}$$

3. Experimental tests

We performed normal contact loading-unloading tests between an optically glass lens and rubber substrates. The spherical glass indenter presents a radius of curvature of 103.7 mm. The rubber substrate is made of PolyDiMethyl-

Siloxane (PDMS). PDMS sample has been manufactured by cross-linking at 70 °C for 24 hours a mixture of Sylgard 184 and Sylgard 527 liquid silicones, with a 0.35 : 0.65 weight ratio.

The glass indenter is fixed to a vertical translation stage by a double cantilever beam, whose deflection allows to measure the contact load. Contact pictures are recorded by using a high-definition camera. The values of the contact radius are then obtained post-processing the images.

The loading phase was performed under controlled load conditions. Contact pictures were taken at fixed load steps. In order to avoid viscoelastic effects, once each load step is reached, contact was maintained for a long time (300 s). This ensures that the adhesive equilibrium is established and static condition is reached.

During unloading, the velocity of the vertical stage is fixed and a constant pull-off rate can be assumed ($V = -d\delta/dt = const$). Moreover, unloading tests were performed at different values of the displacement velocity (V = 0.0002, 0.002, 0.02 mm/s).

Fig. 2 shows an example of evolution of the contact area, captured with the high-definition camera, during the unloading process.

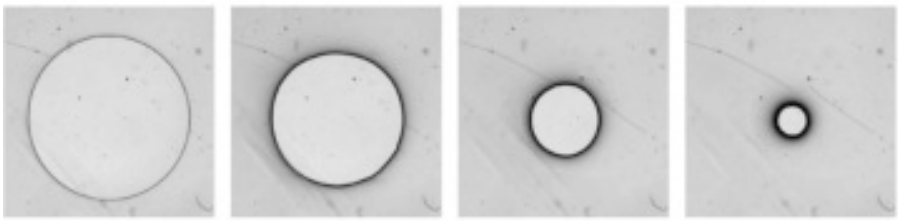

Fig. 2: Contact spot reduction during unloading. The initial load is $\bar{P}_{\max} = 1.17$.

4. Results

Experimental tests were performed by changing the velocity of the indenter during the unloading and investigating also the effect of the load at the end of the loading phase on the pull-off force. The force vs contact radius data were fitted according to JKR theory (loading phase) and Muller numerical solution (unloading phase).

Further, with the values of β and n obtained from the experiments, a numerical study was performed to quantify the elastic and viscoelastic adhesion hysteresis.

The composite elastic modulus ($E^* = 0.827$ MPa) and adhesion energy ($\Delta\gamma_0 = 0.035$ J/m^2) were calculated by fitting, with JKR theory, the contact radius vs load data obtained during the loading phase (Fig. 3).

The unloading phase is instead described by eq. (1) to solve which we need to find the two parameters β and n.

The parameter n can be estimated by exploiting the assumption originally proposed by Gent and Shultz (1972), according to which the effective surface energy $\Delta\gamma$ is related to the velocity of the contact line $v_p = -da/dt$ by

$$\Delta\gamma = \Delta\gamma_0 \left(1 + const \cdot v_p^n\right). \tag{5}$$

The velocity of the contact line $v_p = -da/dt$ is calculated post-processing the images of the contact area captured during the unloading process. Moreover, as shown by Maugis and Barquins (1980), the effective surface energy at equilibrium is equal to the strain energy release rate

$$G = \frac{(P_H - P)^2}{6\pi R P_H} \tag{6}$$

where $P_H = 4E^* a^3/(3R)$ is the Hertzian load and P is the applied load.

Fig. 4 shows the energy release rate G as a function of v_p. Experimental data refer to unloading tests performed at different displacement velocities of the indenter (V = 0.0002, 0.002, 0.02 mm/s). In agreement with previous studies (Maugis and Barquins (1980)), we found that the $\log[G] - \log[v_p]$ relation is linear. In particular, data fitting returns $n \sim 0.2$.

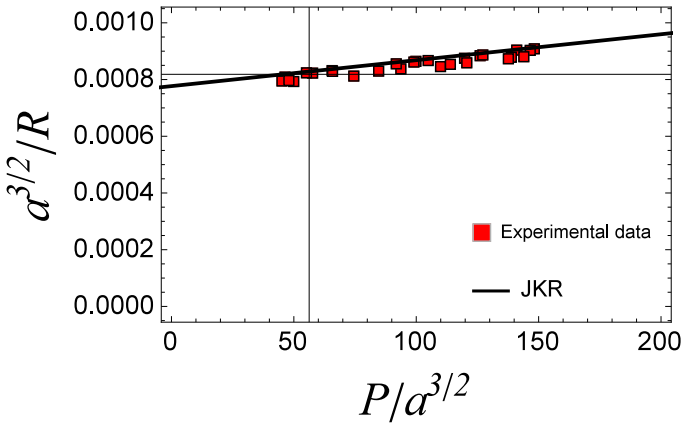

Fig. 3: Contact radius vs force relation obtained during the loading phase. The markers refer to experimental data, the black line to the JKR fit.

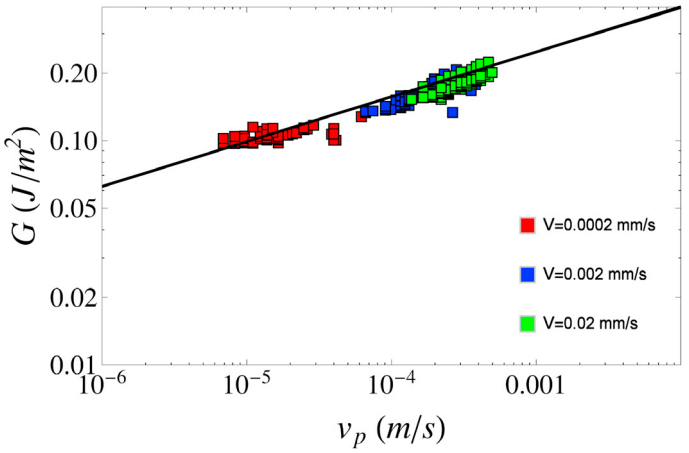

Fig. 4: The strain energy release rate G as a function of the contact line velocity $v_p = -da/dt$. Data refer to experiments performed at different driving velocities of the indenter ($V = 0.0002, 0.002, 0.02$ mm/s). The linear fit returns $n = 0.2$.

The second parameter β can be estimated from the load vs contact radius data measured during the unloading. In this regard, Fig. 5a shows the unloading data obtained by changing the displacement velocity V over three orders of magnitude ($V = 0.0002, 0.002, 0.02$ mm/s). Coloured curves are instead obtained by solving eq. (1) with the values of β that gives the best fit of the experimental data. Notice n is independent of V as it is a characteristic constant of the elastomer. On the contrary, β is proportional to V.

The effect of the maximum force $\bar{P}_{\max}$ reached at the end of the loading phase is investigated in Fig. 5b, for fixed displacement velocity of the indenter $V = 0.002$ mm/s. For smooth surfaces, where complete contact occurs in the region $r \leq a$, we expect the pull-off force to be independent of $\bar{P}_{\max}$ (Dorogin et al. (2017)). Both numerical and experimental data confirm this prediction. In fact, we found a very slight increase in the pull-off force with $\bar{P}_{\max}$ as a result of the stretching of polymer chains occurring before breaking the adhesive bond. This could be the reason of a slight increase in the work of adhesion during pull-off.

Finally, Figs. 6a-b show the pull-off force in terms of the displacement velocity V (Fig. 6a) and maximum load $\bar{P}_{\max}$ (Fig. 6b). As already above predicted, the pull-off force is strongly influenced by V, while negligible effects are observed by changing $\bar{P}_{\max}$. Moreover, the figures show a quite good agreement between experimental values and numerical fit.

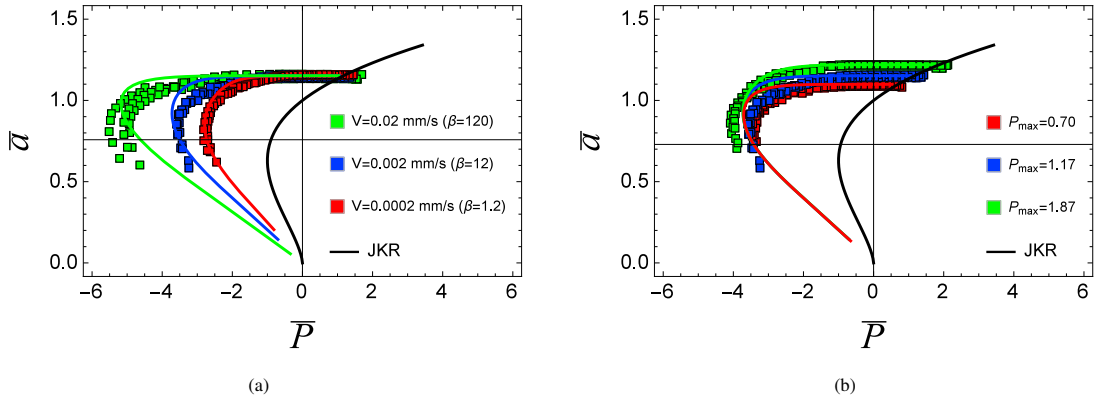

Fig. 5: a) The $\bar{P} - \bar{a}$ relation for different unloading displacement velocities (V = 0.0002, 0.002, 0.02 mm/s). Experimental data (markers) are fitted with the Muller model (solid lines). The value of β used to fit the experimental data are also shown in the figure. The JKR curve is also shown as a reference. b) The $\bar{P} - \bar{a}$ relation for different initial maximum preload ($\bar{P}_{\max}$ = 0.70, 1.17, 1.87). Experimental data (markers) are fitted with the Muller model (solid lines). Experiments are performed at V = 0.002 mm/s. The corresponding value of β is equal to 12. The JKR curve is also shown as a reference.

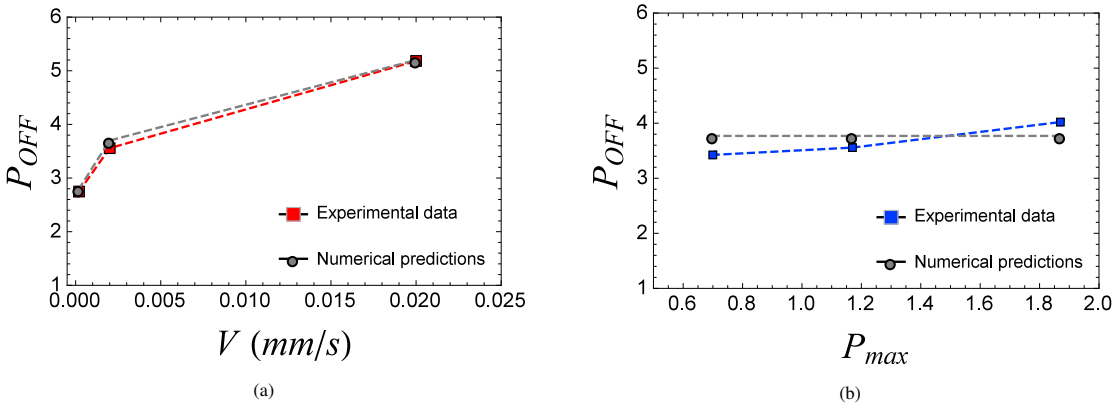

Fig. 6: a) The normalized pull-off force for different unlaoding displacement velocities (V = 0.0002, 0.002, 0.02 mm/s). Experimental data (red squares) are compared with the predictions of Muller's model (gray circles). b) The normalized pull-off force for different maximum preload ($\bar{P}_{\max}$ = 0.70, 1.17, 1.87). Experimental data (blue squares) are compared with the predictions of Muller's model (gray circles).

4.1. Adhesion hysteresis

As above explained, we can separate the energy loss due to elastic instabilities (EAH) from that due to viscoelastic dissipation (VAH) by exploiting a mixed JKR-Muller model.

Fig 7a-b shows the $\bar{P} - \bar{\delta}$ relation for the loading (JKR theory) and unloading (Muller model) process for three different displacement velocities V (Fig. 7a) and maximum load $\bar{P}_{\max}$ (Fig. 7b). Of course, V and $\bar{P}_{\max}$ have no influence on EAH as it depends only on the jump-on and jump-off contact instabilities. The energy loss for EAH corresponds to the yellow area in the figures.

The energy dissipated for viscous effects is instead strongly dependent on the detachement velocity V, but it is practically unaffected by $\bar{P}_{\max}$. It is represented in the figures by the area between the JKR loading curve and the Muller unloading lines.

Tables 1 and 2 summarize the contribution to the energy loss due to VAH with respect to that due to EAH. We found that VAH is not negligible even at very small velocities and increases with V less than proportionally. The slight enhancement observed with $\bar{P}_{\max}$ is probably due to the increase in the adhesion work occuring at pull-off as a result of the polymer chains stretching.

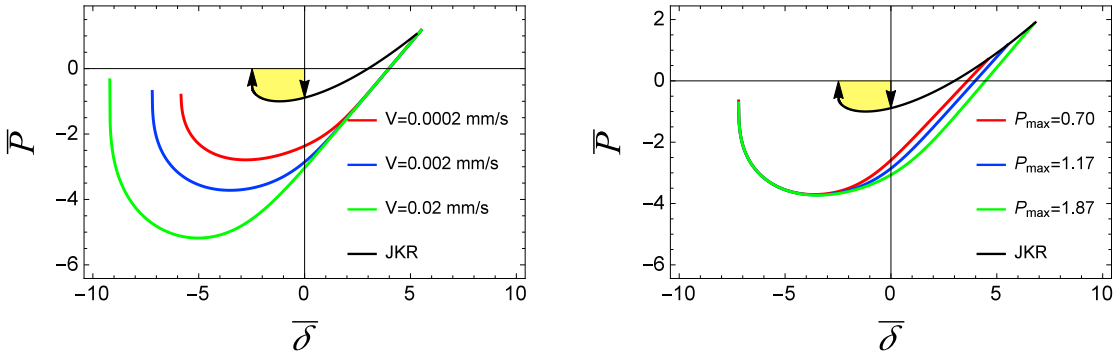

(a) (b)

Fig. 7: a) The $\bar{P} - \bar{\delta}$ relation for different unloading displacement velocities (V = 0.0002, 0.002, 0.02 mm/s). Solid lines refer to Muller's model. The JKR curve is also shown. The energy loss for EAH corresponds to the yellow area. b) The $\bar{P} - \bar{\delta}$ relation for different maximum preload ($\bar{P}_{max}$ = 0.70, 1.17, 1.87). Solid lines refer to Muller's model. The JKR curve is also shown. The energy loss for EAH corresponds to the yellow area.

Table 1. The ratio between the energy loss for VAH and that for EAH for different detachment velocities V.

V(mm/s)	0.0002	0.002	0.02
VAH/EAH	7.36	11.52	18.97

Table 2. The ratio between the energy loss for VAH and that for EAH for different maximum load $\bar{P}_{max}$.

$\bar{P}_{max}$	0.70	1.17	1.87
VAH/EAH	10.76	11.52	12.58

5. Conclusions

In classical works, where the process of attachment-detachment of compliant spheres is investigated from an experimental point of view, the loading-unloading curves are usually fitted by exploiting the classical JKR theory with the stratagem to assume different values of the elastic modulus $E^*$and adhesion energy $\Delta\gamma$ for the loading and unloading phases, respectively.

Here, we adopt a new approach where JKR theory is used to fit the loading data, which are obtained ensuring that adhesive equilibrium is established and static conditions are reached. In such way, we are confident that viscous dissipation is negligible. Unloading data are instead fitted according to the numerical model proposed by Muller (1999), which takes account of the viscoelastic effects occurring during the debonding.

This method allows to calculate accurately the energy loss due to adhesion hysteresis and, in particular, to distinguish the contribution due to elastic instabilities from that due to viscous dissipation. Results show that great viscoelastic adhesion hysteresis may occur in the debonding of elastomers, even if unloading occurs at vwey low velocities (of the order of few micrometer per seconds). However, in this respect, a complete characterization of the material would be necessary to correctly define the range of frequency where the effect of viscous damping is really negligible.

Acknowledgement

GV and LA acknowledge prof. Antoine Chateauminois for his precious help in performing contact experiments at the Soft Matter Sciences and Engineering Laboratory (ESPCI-Paris).

The authors acknowledge support from the Italian Ministry of Education, University and Research (MIUR) under the program "Departments of Excellence" (L.232/2016).

References

Acito, V., Ciavarella, M., Prevost A., & Chateauminois A., 2019. Adhesive contact of model randomly rough rubber surfaces. Tribology Letters, 67: 54. https://doi.org/10.1007/s11249-019-1164-9

Afferrante, L., Carbone, G, & Demelio, G., 2012. Interacting and coalescing Hertzian asperities: A new multiasperity contact model. Wear, 278–279, 28–33. https://doi.org/10.1016/j.wear.2011.12.013

Afferrante, L. & Carbone, G., 2016. The ultratough peeling of elastic tapes from viscoelastic substrates. Journal of the Mechanics and Physics of Solids, 96, 223-234.

Afferrante, L., Bottiglione, F., Putignano, C., Persson, B.N.J., Carbone, G., 2018. Elastic contact mechanics of randomly rough surfaces: an assessment of advanced asperity models and Persson's theory. Tribology Letters, 66, 75. https://doi.org/10.1007/s11249-018-1026-x

Afferrante, L., Putignano, C., Menga, N., & Carbone, G., 2019. Friction in rough contacts of linear viscoelastic surfaces with anisotropic statistical properties. The European Physical Journal E, 42(6), 80.

Attard, P., 2000. Interaction and Deformation of Elastic Bodies: Origin of Adhesion Hysteresis. The Journal of Physical Chemistry B, 104(45), 10635–10641. https://doi.org/10.1021/jp001895

Chen, N., Maeda, N., Tirrell, M., & Israelachvili, J., 2005. Adhesion and friction of polymer surfaces: The effect of chain ends. Macromolecules, 38(8), 3491–3503. https://doi.org/10.1021/ma047733e

Ciavarella, M., Greenwood, J. A., & Barber, J. R., 2017. Effect of Tabor parameter on hysteresis losses during adhesive contact. Journal of the Mechanics and Physics of Solids, 98, 236-244.

Cross, G. L. W., Schirmeisen, A., Grütter, P., & Dürig, U. T., 2006. Plasticity, healing and shakedown in sharp-asperity nanoindentation. Nature Materials, 5(5), 370–376. https://doi.org/10.1038/nmat1632

Derjaguin, B. V., Muller, V. M., & Toporov, Y. P., 1975. Effect of contact deformations on the adhesion of particles. Journal of Colloid And Interface Science, 53(2), 314–326. https://doi.org/10.1016/0021-9797(75)90018-1

Dorogin, L., Tiwari, A., Rotella, C., Mangiagalli, P., & Persson, B. N. J., 2017. Role of preload in adhesion of rough surfaces. Physical review letters, 118(23), 238001.

Gent, A. N., & Schultz, J., 1972. Effect of wetting liquids on the strength of adhesion of viscoelastic material. The Journal of Adhesion, 3(4), 281-294.

Giri, M., Bousfield, D. B., & Unertl, W. N., 2001. Dynamic contacts on viscoelastic films: Work of adhesion. Langmuir, 17(10), 2973–2981. https://doi.org/10.1021/la001565b

Greenwood, J. A., 1997. Adhesion of elastic spheres. Proceedings of the Royal Society of London. Series A: Mathematical, Physical and Engineering Sciences, 453(1961), 1277-1297.

Greenwood, J. A., & Johnson, K. L., 1981. The mechanics of adhesion of viscoelastic solids. Philosophical Magazine A, 43(3), 697-711.

Johnson, K. L., Kendall, K., & Roberts, A. D., 1971. Surface Energy and the Contact of Elastic Solids. Proceedings of the Royal Society A: Mathematical, Physical and Engineering Sciences, 324(1558), 301–313. https://doi.org/10.1098/rspa.1971.0141

Lorenz, B., Krick, B. A., Mulakaluri, N., Smolyakova, M., Dieluweit, S., Sawyer, W. G., & Persson, B. N. J., 2013. Adhesion: Role of bulk viscoelasticity and surface roughness. Journal of Physics Condensed Matter, 25(22). https://doi.org/10.1088/0953-8984/25/22/225004

Maeda, N., Chen, N., Tirrell, M., & Israelachvili, J. N., 2002. Adhesion and friction mechanisms of polymer-on-polymer surfaces. Science, 297(5580), 379–382. https://doi.org/10.1126/science.1072378

Maugis, D., & Barquins, M., 1980. Fracture mechanics and adherence of viscoelastic solids. In Adhesion and adsorption of polymers (pp. 203-277). Springer, Boston, MA.

Menga, N., Afferrante, L., & Carbone, G., 2018. Effect of thickness and boundary conditions on the behavior of viscoelastic layers in sliding contact with wavy profiles. Journal of the Mechanics and Physics of Solids, 95, 517-529.

Menga, N., Afferrante, L., Demelio, G., & Carbone, G., 2018. Rough contact of sliding viscoelastic layers: numerical calculations and theoretical predictions. Tribology International, 122, 67–75.

Muller, V. M., 1999. On the theory of pull-off of a viscoelastic sphere from a flat surface. Journal of Adhesion Science and Technology, 13(9), 999-1016.

Oliver, W. C., & Pharr, G. M., 1992. An improved technique for determining hardness and elastic modulus using load and displacement sensing indentation experiments. Journal of materials research, 7(6), 1564-1583.

Putignano, C., Menga, N., Afferrante, L., & Carbone, G., 2019. Viscoelasticity induces anisotropy in contacts of rough solids. Journal of the Mechanics and Physics of Solids, 129, 147-159.

Tabor, D., 1977. Surface forces and surface interactions. Journal of Colloid And Interface Science, 58(1), 2-13. https://doi.org/10.1016/0021-9797(77)90366-6

Tiwari, A., Dorogin, L., Bennett, A. I., Schulze, K. D., Sawyer, W. G., Tahir, M., ... & Persson, B. N. J., 2017. The effect of surface roughness and viscoelasticity on rubber adhesion. Soft Matter, 13(19), 3602-3621.

Violano, G., Demelio, G.P., & Afferrante, L., 2018.On the DMT adhesion theory: From the first studies to the modern applications in rough contacts. Procedia Structural Integrity, 12, 58-70. https://doi.org/10.1016/j.prostr.2018.11.106

Violano, G., & Afferrante, L., 2019. On DMT methods to calculate adhesion in rough contacts. Tribology International, 130, 36-42. https://doi.org/10.1016/j.triboint.2018.09.004

Violano, G., & Afferrante, L., 2019. Contact of rough surfaces: modeling adhesion in advanced multiasperity models. Part J: Journal of Engineering Tribology. https://doi.org/10.1177/1350650119838669

Yashima, S., Romero, V., Wandersman, E., Fretigny, C., Chaudhury, M. K., Chateauminois, A., & Prevost, A. M., 2015. Normal contact and friction of rubber with model randomly rough surfaces. Soft Matter, 11(5), 871-881.